Proceedings of the Estonian Academy of Sciences,
2021, **70**, 4, 516–523
https://doi.org/10.3176/proc.2021.4.20
Available online at www.eap.ee/proceedings

MATERIALS
ENGINEERING

Thermal analysis of the friction stir welding process based on boundary conditions and operating parameters

Moustafa Boukraa[a], David Bassir[b,c*], Nadhir Lebaal[d], Tawfiq Chekifi[a], Mouloud Aissani[a], Nacer Tal Ighil[a] and Amina Mataoui[e]

[a] Research Center in Industrial Technologies CRTI, P.O. Box 64, Cheraga 16014, Algiers, Algeria
[b] Université Bourgogne Franche-Comté, UTBM, UMR CNRS 6303, 90010 Belfort, France
[c] Centre Borelli, ENS-University of Paris-Saclay, 91190 Gif-sur-Yvette, France
[d] Université Bourgogne Franche-Comté, UTBM, ICB Lab., France
[e] Theoretical and Applied Laboratory of Fluid Mechanics, USTHB, Algiers, Algeria

Received 16 September 2021, accepted 22 October 2021, available online 11 November 2021

Abstract. Modelling of friction stir welding (FSW) remains a complicated task, as it is crucial to predict the mechanical properties of the final welded part. This research focuses on the numerical simulation aspect of the alloy material AA2195-T8. 3D transient thermal model was applied to simulate the heat transfer phenomena in the welding phase. In this model, the FSW tool is considered as a circular heat source moving in a rectangular plate having a cooling surface and subjected to non-uniform and non-homogeneous boundary conditions. To solve the thermal problem, the finite element method was used as part of a Lagrangian formulation. The obtained results allow us to determine the maximum value of the temperature in the Nugget zone of the welded joint. Sensitivity analysis of the operating parameters was also investigated to determine the thermal cycle and the temperature distribution during this welding process. Our results were successfully compared with the ones available in the literature with good agreement.

Key words: friction stir welding, heat transfer, finite element method, AA2195-T8, alloy material, parameter characterisation.

INTRODUCTION

Several industries such as aeronautics, aerospace and automotive industries benefit from the use of structurally hardened aluminium alloys as it presents a major advantage. Structural engineers require materials that will allow them to design lightweight, cost-effective structures that have good durability and damage tolerance. However, the difficulty of assembling those structures through fusion welding techniques (TIG, MIG-MAG...) remains a crucial problem. A solid-state welding technique [1–3] was introduced almost three decades ago by the Welding Institute (TWI) in the United Kingdom in 1991. This technique is called the friction stir welding (FSW) process and it consists in using a specific rotational tool *(formed by a shoulder and a shaped probe)* to provide required weld properties [4]. The heat energy requires to join the two sides of the plates *(retreating side RS and advancing side AS respectively)* [5]. Heat is generated by the friction between the rotating tool and the mentioned surface as described in Fig. 1. In the last decade, many researchers have investigated numerically and experimentally how to optimize the FSW technique – in particular, the heat transfer phenomena and material flow [6,7]. It was underlined in different literature sources that the perpendicular distribution of temperature is nearly isothermal under the shoulder tool. Moreover, increasing the pressure and the rotational speed enhances the maximum value of welding temperature.

* Corresponding author, david.bassir@utbm.fr

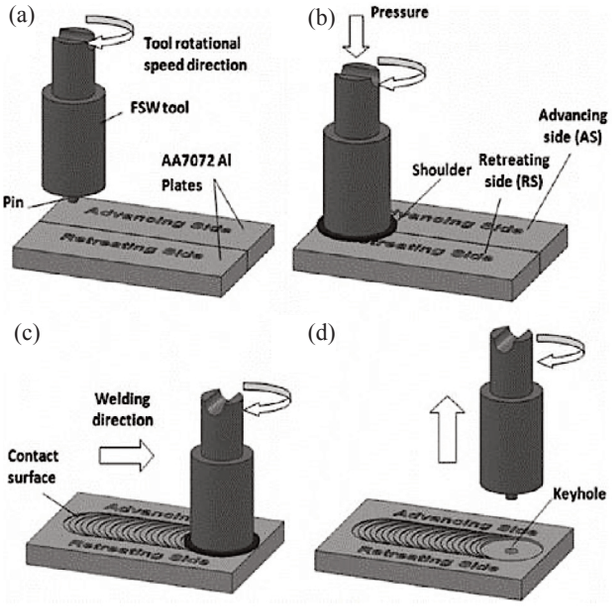

Fig. 1. Presentation of the different steps of the FSW process: (a) start, (b) penetration, (c) welding and (d) finishing [3].

It is important to mention that inadequate heat generation in this welding process could lead to failure of the tool-probe or the workpiece shape [8,9]. Thus, understanding the heat flow behaviour is important to achieve good welding [2,4,5,10]. Simar et al. [11] determined the thermal history experimentally at positions near the weld line during the FSW process. Also, they developed a numerical model based on the finite element method (FEM), considering the effect of the welding parameters such as the welding speed, tool rotational speed, axial force and tool geometry. Moraitis et al. [12] calculated by using semi-analytical methods the total energy and the heat produced by stirring the material during the FSW process. They also proposed a 3D numerical simulation to analyse the thermal histories during the welding process. The obtained results were introduced into a thermo-mechanical model to determine the residual stress. The results were afterward validated experimentally. In a recent study [13,14], the authors analysed experimentally and numerically the thermo-mechanical behaviour of FSW for a PMMA plate. Their objective was to seek for suitable conditions to attain optimal thermomechanical properties. The developed model was used to determine the thermal profile in the longitudinal and transverse directions of the welded plates, while the temperature of the surface plate was measured experimentally and compared to the simulation. The authors underlined that at higher heat inputs, with the increased axial force within the plastic material, it led to the material sticking around the probe and to the formation of defects.

In this work, a numerical simulation of the FSW process was carried out, making it possible to study the thermal phenomena as well as the heat transfer. A 3D thermal model was applied in order to consider the thermal transient, whereby the welding tool was regarded as a mobile heat source. The effect of boundary conditions and the operating parameters (*welding speed, rotational speed, axial force and probe radius*) on the heat transfer during the welding process were investigated.

2. PHYSICAL MODEL AND NUMERICAL SIMULATION

The workpiece is composed of two plates to be welded by the FSW process, its dimensions are $L \times W \times H = 610 \times 102 \times 8.1$ mm^3 (Fig. 2a). The intersection of the workpiece with the FSW tool is represented by a circular red section that moves throughout the weld joint line. To complete the

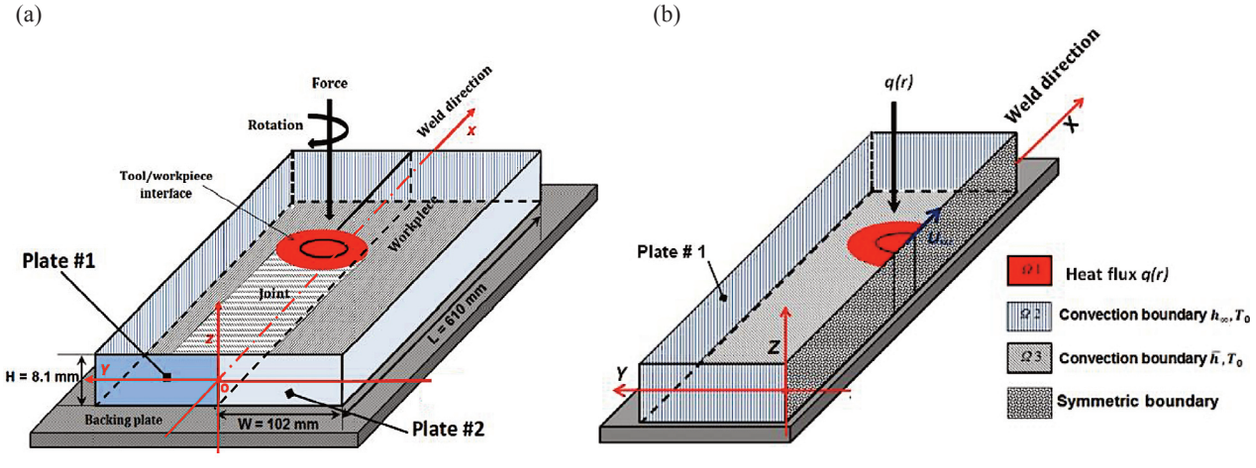

Fig. 2. Applied heat transfer boundary conditions on the computational domain.

mathematical model presented in the next session, the boundary conditions were also specified. Since the plates were made from the same material (*aluminium alloy*) and had similar dimensions, symmetric condition was applied along the joint, so the calculation was performed on one side (Fig. 2b).

2.1. Mathematical model

The modelling of the FSW heat phenomena is based on the resolution of the heat conduction equation in the workpiece with an appropriate model of the heat source. In this research, a modified heat source Q_{source} was used for the friction effects of the welding tool on the workpiece, taking into account the appropriate boundary and initial conditions [3].

2.2. Hypothesis

Some hypotheses were necessary to solve the obtained system:

- The heat transfer process is considered 3D and transient in the entire workpiece;
- The peak temperature in the workpiece during the welding remains always below the melting temperature of the studied material (T_m below 773 K);
- The heat exchange between the workpiece and the environment occurs only through a natural convection process with a heat coefficient h_∞ and radiation effect during the process is neglected;
- The heat due to the plastic deformation of the material by the FSW tool is neglected compared to the heat generated by the rotational friction;
- The force applied vertically by the welding tool generates a uniform pressure at the workpiece/shoulder interface.

2.3. Heat transfer equation

The tool moves at constant speed $\boldsymbol{u_w}$ along the joint line according to the above assumptions. The thermal energy equation in the workpiece can be written in the Lagrangian coordinates as:

$$\rho(T)c_p(T)\frac{\partial T}{\partial t} = \nabla(K.\nabla T) + S\,, \tag{1}$$

where

- $\boldsymbol{\rho}(T)$, $\boldsymbol{c_p}(T)$ *and* $\boldsymbol{K}$(*kx, ky, kz*) *are the material density, the thermal capacity and the thermal conductivity, which depend on temperature;*
- *S is the volumetric heat source due to the plastic deformation of the material. It is often neglected compared to the main source of the heat created by the friction of the shoulder* $\boldsymbol{q_s}$ *and the probe* $\boldsymbol{q_p}$ *on the workpiece*.

In the FSW process, the heat is directly linked to the contact conditions of the *workpiece/tool interfaces* and the process parameters. Therefore, there are two main sources of energy produced by friction at the two interfaces: the heat $\boldsymbol{Q_p}$ created at the *workpiece/probe interface* and the heat $\boldsymbol{Q_s}$ created at the *workpiece/shoulder interface*. These frictional contacts depend on the surface state, which is defined by the friction coefficient $\boldsymbol{\mu}$. Our model is based on the model of Chao at al. [15] (Fig. 3) as follows:

$$q(r) = \frac{3Q_{source}}{2\pi R_S^3} r \;\text{ for }\; r \le R_S\,, \tag{2}$$

$$Q_{source} = \frac{\pi^2 \omega P}{45}\mu\left(R_S^3 + 3R_P^2 h_p\right), \tag{3}$$

where

$\boldsymbol{q}(\boldsymbol{r})$ *is the heat flux source,* $\boldsymbol{R_s}$ and $\boldsymbol{R_p}$ are the shoulder and probe radii, $\boldsymbol{P}$ denotes the pressure, $\boldsymbol{\mu}$ is the friction coefficient, $\boldsymbol{\omega}$ rotational speed and $\boldsymbol{h_p}$ refers to the height of the tool probe [3].

3. NUMERICAL PRODECURE AND VALIDATION

The numerical calculation of the temperature fields during the FSW process was performed by CFD-ANSYS software using 391936 finite elements, which requires the resolution of the governing equations by combining the appropriate boundary conditions and a moving heat source. To perform the numerical resolution of the problem and validate the thermal model, it is important to provide experimental data (*operating parameters in Table 1 and observed thermal cycles in reference* [15]).

The material tool is M2 steel, which is widely used in industries. It has small and distributed carbides, giving the tool high wear resistance. The evolution of the temperature at *P1* (*L/2, 12.7, H/4*) and *P2* (*L/2, 25.4, H/4*) is described in Fig. 3. It can be observed that the temperature

Table 1. Properties of the cutting tool materials investigated [6]

Probe radius	Shoulder radius	Rotational speed	Welding speed	Axial force
5 mm	12.7 mm	240 tr/min	2.36 mm/s	25 kN

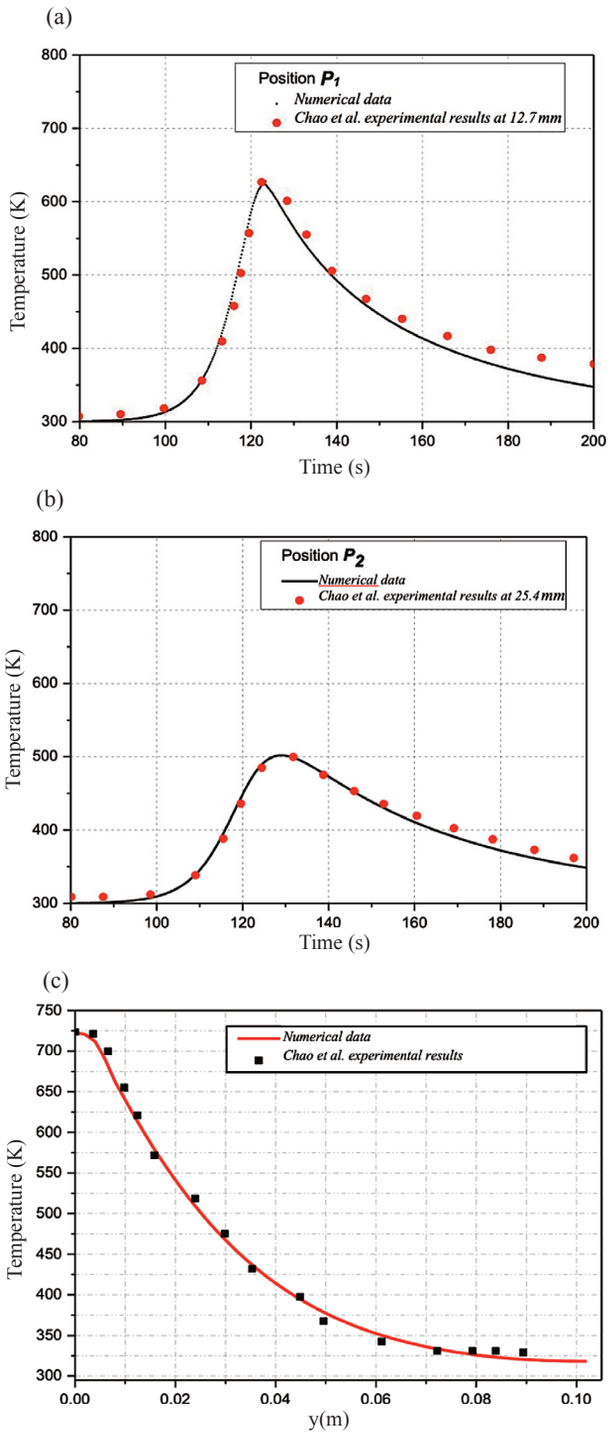

Fig. 3. Comparison of the numerical thermal histories obtained by Chao et al. [15]: the experimental results at two positions of the workpiece (a) P (L/2, 12.7, H/4) and (b) P (L/2, 25.4, H/4), as well as along the (y) line that is perpendicular to the weld line (c).

pick decreases with the increase of distance regarding the mid plan for both experimental and numerical analyses. Based on the good agreement between the simulation and the experiment, the proposed model can be used to predict the temperature profiles and cooling rates.

The results presented in Fig. 3 confirm the fast temperature increase in welded plates followed by slow cooling down. They also show a small difference in the cooling phase between numerical and experimental data due to the fact that the model does not take into account coupling with other phenomena such as the material flow, mechanical deformations and radiation of the heat with the ambient environment. It is also related to measurements of uncertainties (Uncertainty of sensors) as well as to the gap between the real position of the sensors and their location in the FE meshing.

4. RESULTS AND DISCUSSION

The results based on the predictive numerical model fit well with the available experimental measurements. The influence of the welding parameters such as the speed of advance, rotational speed and the diameter of the welding tool on thermal cycling as well as temperature distribution in the workpiece were investigated.

4.1. Temperature distribution

In Fig. 4 the contours of the temperatures in the plane perpendicular to the welding line during the FSW process are shown. These contours were obtained at longitudinal positions X = 0.305 m of the workpiece, for the welding speed values of *1.5 mm/s, 3 mm/s and 4.5 mm/s* and the rotational speed values of *300 tr/min, 400 tr/min and 500 tr/min*. It can be noticed that the temperature at a section increases rapidly when the tool passes through this point for the three cases studied. Meanwhile, the temperature decreases as the welding speed of the tool increases. Moreover, it is clearly observed that the lines of the isotherms are retracted towards the rotation axis of the welding tool when increasing the welding speed. The heat-affected zone near the welding tool is larger when the welding speed decreases because it has more time to conduct heat around the area.

Increasing the rotational speed from 300 to 500 tr/min leads to an increase in the welding heat input, the maximum value of the temperature and the overall level of the temperature. The distance between the peak temperatures of the contour 523 K (250 °C) and the *shoulder/workpiece interface* increases as well.

4.2. Effect of the heat transfer coefficient h_{inf} and h_{lat}

Figure 5 shows the temperature distribution in the plane perpendicular to the welding direction for the following

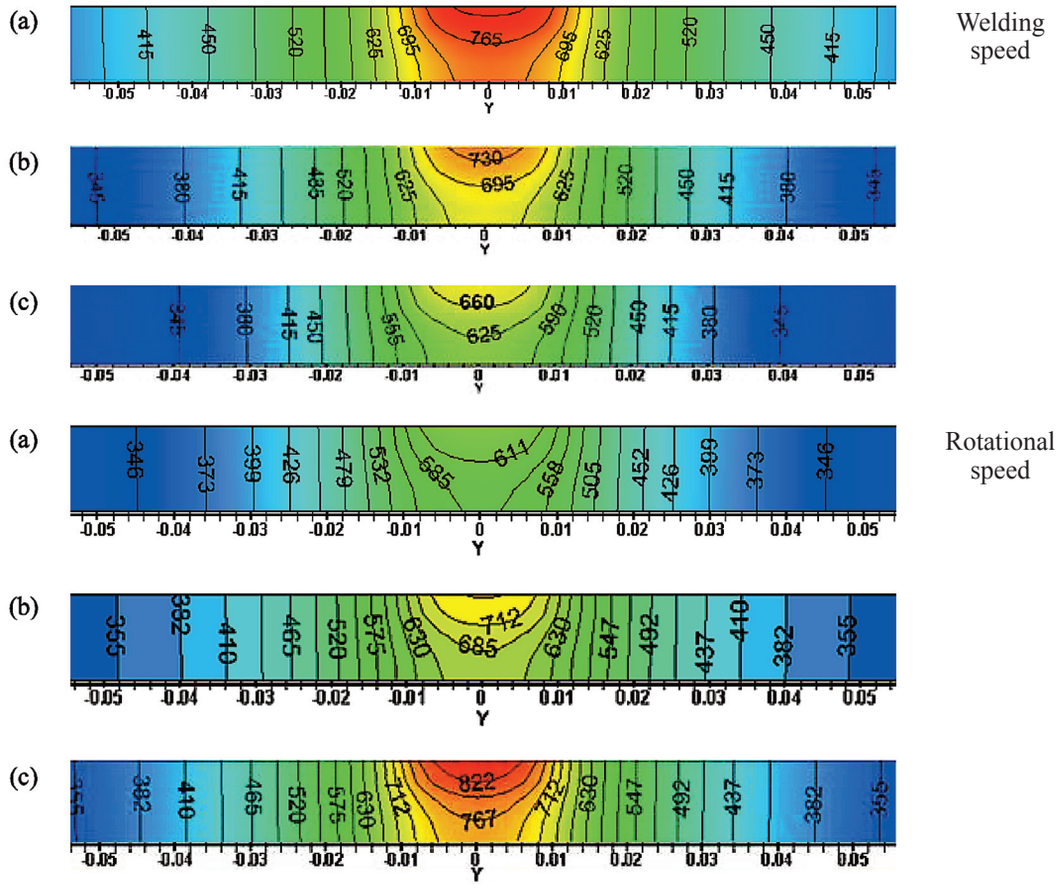

Fig. 4. Effect of welding speed and rotational speed on the temperature field in the plane perpendicular to the welding line: (a) 1.5 mm/s, (b) 3.0 mm/s, (c) 4.5 mm/s ((a) 300 tr/min, (b) 400 tr/min, (c) 500 tr/min).

parameters of the welding process: $u_w = 3$ *mm/s,* $w =$ *400 tr/min,* $F = 15$ *kN and* $R_S = 12.7$ *mm.*

When h_{lat} increases, the hottest zone of the workpiece will be located more and more around the welding tool. The calculations with different h_{inf} values were made at the workpiece/backing interface and with the same operating parameters previously used for h_{lat}. The same effect is observed for h_{lat} – when h_{inf} increased, the maximum value of the temperature at the *tool/workpiece interface* to be welded was slightly reduced, as was the hottest zone around the tool.

4.2. Thermal cycles

Figure 6a, 6b and 6c shows the thermal cycles at point P1 ($x = 305$ mm, $y = 12.7$ mm, $z = 2$ mm) for three welding speeds (1.5, 3.0 and 4.5 mm/s), for three rotational speeds (300, 400 and 500 tr/min) and for three tool shoulder diameters (10, 12.7 and 15 mm), respectively. For the three values of the welding speed (Fig. 6a), very rapid variations in the temperature are observed during the passage of the tool. These variations are represented by a rapid increase in temperature (heating phase) up to the maximum value at the time of the passage of the welding tool by position P1; father from this, the temperature decreases to a uniform value of 320 K (cooling phase). When the welding speed is doubled or tripled, the maximum temperature value decreases to 68.5 °C and 122.6 °C, respectively. This difference in terms of temperature is due to the rate of the amount of heat dissipated in the workpiece.

The rotational speed is a significant variable that influences the thermal cycle through the FSW process. When the rotational speed increases, the temperature gradient increases to the maximum value, almost identical with the heating time ($t = 96$ s). Also, the thermal cycle obtained for the rotational speed of 300 tr/min has a higher cooling speed compared to the other cases (Fig. 6b). In addition, a larger shoulder increases the quantity of heat created by the friction, but also results in a greater quantity of entrained material. This implies an increase in the amount of heat generated, as shown in Fig. 6c for the three values of shoulder diameter tools of 10 mm, 12.7 mm and 15 mm.

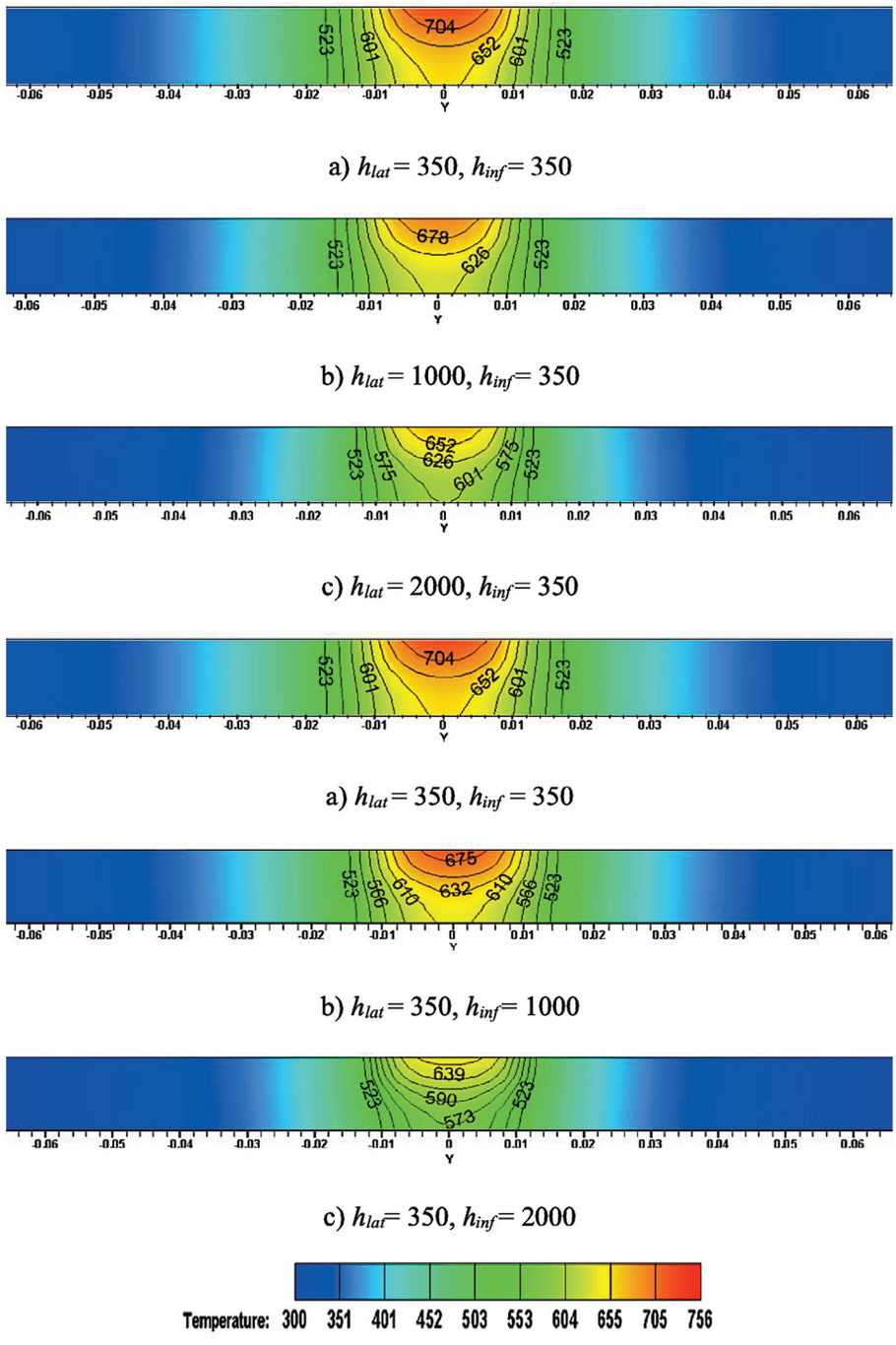

Fig. 5. Effect of h_{lat} and h_{inf} on the thermal field in the plane perpendicular to the welding direction at x = 305 mm (u_w = *3 mm/s, w = 400 tr/min, F = 15 kN, R_S = 12.7 mm*).

5. CONCLUSIONS

In this research, a transient thermal model for friction stir welding process was used with a good prediction of the temperature distribution, the temperature profiles and the cooling rates compared to the experimental data available in the literature. The three-dimensional model that was developed with the alloy material AA2195-T8 can be easily coupled with an optimization method [16] to improve the welding process and reduce further the manufacturing cost. A microscopic study around the weld area with fatigue testing would allow us to consolidate our numerical approach and to predict the damage at the first level.

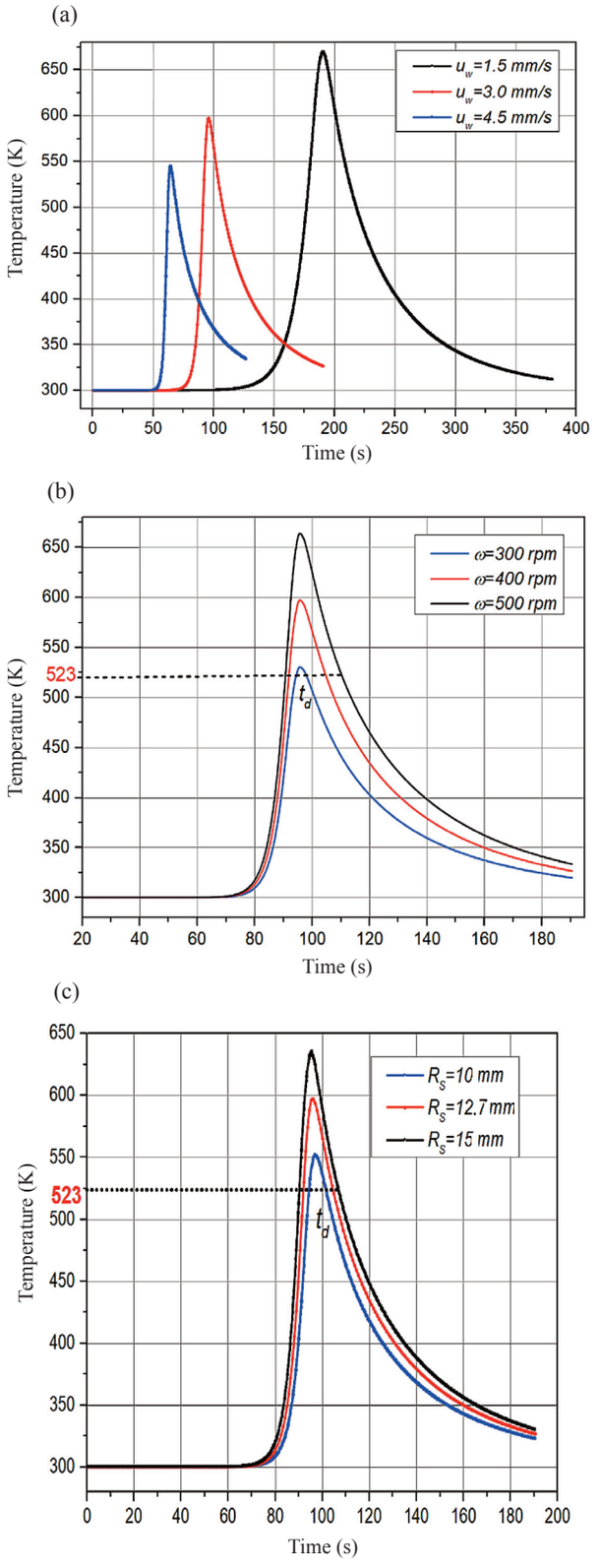

Fig. 6. Effect of the welding parameters: (a) welding speed, (b) rotational speed of the tool and (c) diameter of the tool shoulder on thermal cycles at point P_1 (*x = 305 mm, y = 12.7 mm, z = 2 mm*).

ACKNOWLEDGEMENTS

The publication costs of this article were covered by the Estonian Academy of Sciences and Tallinn University of Technology.

REFERENCES

1. Verma, S. and Misra, J. P. A critical review of friction stir welding process. In *DAAM International Scientific Book* (Katalinic, B., ed.). DAAM International, Vienna, 2015, 249–266.
2. Nandan, R., DebRoy, T. and Bhadeshia, H. K. D. H. Recent advances in friction-stir welding – Process, weldment structure and properties. *Prog. Mater. Sci.*, 2008, **53**(6), 980–1023. https://doi.org/10.1016/j.pmatsci.2008.05.001
3. Aissani, M., Guessasma, S., Zitouni, A., Hamzaoui, R., Bassir, D. and Benkedda, Y. Three-dimensional simulation of 304L steel TIG welding process: Contribution of the thermal flux. *Appl. Therm. Eng.*, 2015, **85**, 822–832. https://doi.org/10.1016/j.applthermaleng.2015.06.035
4. Hassan, A. S., Mahmoud, T. S., Mahmoud, F. H. and Khalifa, T. A. Friction stir welding of dissimilar A319 and A356 aluminium cast alloys. *Sci. Technol. Weld. Join.*, 2010, **15**(5), 414–422. https://doi.org/10.1179/136217110X12720264008358
5. Sun, Z., Wu, C. S. and Kumar, S. Determination of heat generation by correlating the interfacial friction stress with temperature in friction stir welding. *J. Manuf. Process.*, 2018, **31**, 801–811. https://doi.org/10.1016/j.jmapro.2018.01.010
6. Gibson, B. T., Lammlein, D. H., Prater, T. J., Longhurst, W. R., Cox, C. D., Ballun, M. C. et al. Friction stir welding: Process, automation, and control. *J. Manuf. Process*, 2014, **16**(1), 56–73. https://doi.org/10.1016/j.jmapro.2013.04.002
7. Taysom, B. S., Sorensen, C. D. and Hedengren, J. D. A comparison of model predictive control and PID temperature control in friction stir welding. *J. Manuf. Process.*, 2017, **29**, 232–241. https://doi.org/10.1016/j.jmapro.2017.07.015
8. Lakshmi Balasubramaniam, G., Boldsaikhan, E., Fukada, S., Fujimoto, M. and Kamimuki, K. Effects of refill friction stir spot weld spacing and edge margin on mechanical properties of multi-spot-welded panels. *J. Manuf. Mater. Process.*, 2020, **4**(2), 55. https://doi.org/10.3390/jmmp4020055
9. Boukraa, M., Lebaal, N., Mataoui, A., Settar, A., Aissani, M. and Tala-Ighil, N. Friction stir welding process improvement through coupling an optimization procedure and three-dimensional transient heat transfer numerical analysis. *J. Manuf. Process.*, 2018, **34**(Part A), 566–578. https://doi.org/10.1016/j.jmapro.2018.07.002
10. Singh, K., Singh, G. and Singh, H. Review on friction stir welding of magnesium alloys. *J. Magnes. Alloys*, 2018, **6**(4), 399–416. https://doi.org/10.1016/j.jma.2018.06.001
11. Netto, N., Zhao, L., Soete, J., Pyka, G. and Simar, A. Manufacturing high strength aluminum matrix composites by friction stir processing: An innovative approach. *J. Mater. Process. Technol.*, 2020, **283**, 116722. https://doi.org/10.1016/j.jmatprotec.2020.116722
12. Moraitis, G. A. and Labeas, G. N. Investigation of friction stir welding process with emphasis on calculation of heat

generated due to material stirring. *Sci. Technol. Weld. Join.*, 2010, **15**(2), 177–184. https://doi.org/10.1179/136217109X12537145658779
13. Derazkola, H. A., Khodabakhshi, F. and Simchi, A. Friction-stir lap-joining of aluminium-magnesium/polymethyl-methacrylate hybrid structures: thermo-mechanical modelling and experimental feasibility study. *Sci. Technol. Weld. Join.*, 2018, **23**(1), 35–49. https://doi.org/10.1080/13621718.2017.1323441
14. Derazkola, H. A. and Khodabakhshi, F. Development of fed friction-stir (FFS) process for dissimilar nanocomposite welding between AA2024 aluminum alloy and polycarbonate (PC). *J. Manuf. Process.*, 2020, **54**, 262–273. https://doi.org/10.1016/j.jmapro.2020.03.020
15. Chao, Y. J., Qi, X. and Tang, W. Heat transfer in friction stir welding – Experimental and numerical studies. *J. Manuf. Sci. Eng.*, 2003, **125**(1), 138–145. https://doi.org/10.1115/1.1537741
16. Majak, J., Shvartsman, B., Pohlak, M., Karjust, K., Eerme, M. and Tungel, E. Solution of fractional order differential equation by the Haar Wavelet method. Numerical convergence analysis for most commonly used approach. *AIP Conf. Proc.*, 2016, **1738**(1), 480110. https://doi.org/10.1063/1.4952346

Otshõõrdkeevitamise termiline analüüs ääretingimuste ja protsessi parameetrite põhjal

Moustafa Boukraa, David Bassir, Nadhir Lebaal, Tawfiq Chekifi, Mouloud Aissani, Nacer Tal Ighil ja Amina Mataoui

Otshõõrdkeevitamise modelleerimine on jätkuvalt keeruline ülesanne, mille eesmärk on ennustada keevitatud lõpptoote mehaanilisi omadusi. Käesolev uuring keskendub sulami AA2195-T8 numbrilise simuleerimise aspektile. Selleks et simuleerida soojusülekande nähtust keevitamise faasis, rakendatakse ruumilist (3D) transientset termomudelit, kus otshõõrdkeevituse tööriista vaadeldakse kui tsirkulaarset soojusallikat, mis liigub ristküliku kujulise plaadi sees. Plaadil on jahutav pind, mis funktsioneerib ebaühtlastes ja heterogeensetes ääretingimustes. Selleks, et lahendada keevise temperatuurist sõltuvat kvaliteedi ülesannet, kasutatakse lõplike elementide meetodit kui osa Lagrange'i võrrandist. Saadud tulemused võimaldavad määrata kõrgeimat temperatuuri keevisõmbluse tuuma tsoonis. Samuti analüüsitakse protsessi parameetrite tundlikkust selleks, et määrata termilist tsüklit ja temperatuuri jaotust keevitusprotsessis. Käesoleva uuringu tulemused on varem kirjanduses avaldatutega heas kooskõlas.